



## Imparting high-temperature grain stability to an Al-Mg alloy

Abhishek Pariyar<sup>a,b,\*</sup>, Laszlo S. Toth<sup>b,c</sup>, Satish V. Kailas<sup>a</sup>, Laurent Peltier<sup>c</sup>

<sup>a</sup>Department of Mechanical Engineering, Indian Institute of Science, Bangalore 560012, India

<sup>b</sup>Laboratory of Excellence on Design of Alloy Metals for Low-Mass Structure (Labex-DAMAS), Université de Lorraine, 57070 Metz, France

<sup>c</sup>LEM3 Laboratory, Université de Lorraine, CNRS, Arts et Métiers ParisTech, F-57000 Metz, France



### ARTICLE INFO

#### Article history:

Received 25 March 2020

Revised 15 August 2020

Accepted 17 August 2020

Available online 8 September 2020

#### Keywords:

Grain stability

Zener pinning

Aluminum alloy

Hardness

Equiaxed microstructure

### ABSTRACT

Al alloys, despite their excellent strength-to-weight ratio, cannot be used at elevated temperatures because of microstructural instability owing to grain growth and precipitate coarsening, thus, leading to a drastic loss in their strength. In this work, we have attempted to address the issue of grain growth by introducing in-situ formed polymer derived ceramics in an Al-Mg alloy. A stable grain structure with minimal loss in hardness when exposed to 450°C and 550°C for 1 hour was obtained due to the particle pinning of the grain boundaries by the Zener mechanism.

© 2020 Acta Materialia Inc. Published by Elsevier Ltd. All rights reserved.

Al alloys have widespread applications in the aerospace, automotive and shipping industries because of their excellent strength-to-weight ratio compared to other alloys [1,2]. However, most Al alloys cannot sustain their strength at high temperatures, except for a few, like L1<sub>2</sub> phase forming alloys, which can be used till 343°C [3–6]. One of the reasons for this reduction in strength is due to the increase in grain size when exposed to such temperatures.

As explained by the Hall-Petch relationship, the strength of a material increases with the decrease in grain size [7,8]. However, there is also an increase in the grain boundary area per unit volume with a decrease in grain size. It has been shown by Humphreys and Hatherley that if a cube shape is assumed for a grain, reducing the thickness of a sheet in rolling by 50% leads to an increase in the surface area of the grain by ~16%, whereas, reducing it by 99% increases the surface area by ~3267% [9,10]. Decreasing the grain size leads to an increase in the free energy of the system, which makes the microstructure unstable. The grains tend to grow in order to minimize this energy by reducing the grain boundary area per unit volume [10]. Further, the rate of grain growth also increases with the increase in temperature [11].

One way to solve the problem of grain stability in aluminum alloys at high temperatures is by dispersing second phase particles within the Al alloy matrix. Such particles, when present at the grain boundaries, apply a retarding/drag force on their movement

when exposed to high temperatures. This inhibits further motion of the grain boundaries which prevents grain growth by the well-known Zener pinning mechanism. It has been estimated that the Zener pinning effect becomes more pronounced with a decrease in the particle size and increase in their volume fraction [9,11]. However, this mechanism is not active for precipitation hardening Al alloys, because the precipitates coarsen or dissolve at high temperatures. This causes the strength to drop due to recrystallization, grain growth and by the reduction in the number of dislocation barriers. However, the Zener mechanism can also be activated in both precipitation hardening and work hardening Al alloys, by introducing second phase particles, such as ceramics, which are not part of the alloy system [12,13]. It is beneficial to use nano-sized ceramic particles as reinforcements because Zener pinning is more effective with the decrease in the particle size. However, using such particles have issues related to their agglomeration within the matrix. In addition to that, they also raise the manufacturing costs and are potentially hazardous to health during handling due to their nano-size [14]. Further, the breaking of ceramic particles below a particular size is difficult as there is a reduction in the defect density with a decrease in the particle size, making the fracture of ceramic particles progressively more difficult.

Ceramics can also be obtained from special types of polymers that are readily available. These polymers can be pyrolyzed into ceramic particles. Such polymers contain inorganic elements in their main polymeric chain along with organic components on their branches. Most of the organic components are released as volatiles during pyrolysis and the remaining part forms the amorphous ceramics (called polymer derived ceramics (PDCs))

\* Corresponding author at:

E-mail address: [abhishek@iisc.ac.in](mailto:abhishek@iisc.ac.in) (A. Pariyar).

**Table 1**

Chemical composition of the as-received Al 5052 alloy.

Element	Al	Mg	Si	Cr	Mn	Fe	Cu	Zn
Wt.%	96.2	2.81	0.15	0.31	0.10	0.26	0.10	0.06

[15]. Such polymers can be easily broken into nanoscale size, due to their low fracture toughness, by severe plastic deformation methods, especially by high shear processes (e.g. friction stir processing), and can be dispersed within the alloy matrix. Then, by heating to their pyrolysis temperature, the nanosized polymer can be converted into nanosized ceramics in-situ within the alloy. PDCs have very high temperature stability as they are ceramics and can potentially pin the grain boundaries even at high temperatures. Hence, in this work, an attempt has been made to impart high temperature grain stability to an Al-Mg alloy by introducing second phase particles in the form of in-situ polymer derived ceramics using friction stir processing. The particles aided in pinning the grain boundaries and maintaining their stability even at  $0.85 T_m$  with minimal loss in hardness.

The matrix material chosen was Al 5052-H32 sheet (composition shown in Table 1) of 6 mm thickness which was annealed at 343°C for 2 hrs prior to processing. The polymer used was poly-methylhydrosiloxane (PMHS) (Sigma-Aldrich) in the liquid state. The liquid polymer was first cross-linked at room temperature for 8 hrs into a rigid solid structure by adding 5 wt.% 1,4-diazabicyclo[2.2.2] octane (Sigma-Aldrich). The cross-linked polymer was then subjected to ball milling for 60 minutes. The ball-milled polymer powder was filled into grooves of width 3 mm and depth of 4 mm in the Al 5052-O plates. Friction stir processing (FSP) [16] was performed on the plates in order to disperse the polymer particles within the matrix using a hot die steel tool in H13 hardened condition having a conical pin with double start threads. The tool pin length was 5 mm, the diameter at the base was 10 mm, the diameter at the tip was 8 mm, and the shoulder diameter was 25 mm with a chamfer angle of 20°. Three back-to-back passes were performed initially at a tilt angle of 2° using 500 RPM tool rotation speed and 12 mm/min traverse speed. The plunge depths were 5.3 mm, 5.4 mm and 5.5 mm for the first, second and third passes, respectively. After the third pass, the whole plate was put for pyrolyzing the polymer in a furnace at 500°C for 10 hrs. Subsequently, a fourth pass with the same experimental conditions, but using a plunge depth of 5.6 mm, was performed in order to close the pores formed due to the emission of gases during the pyrolysis of the polymer. For thermal stability tests, different specimens of the same material state were subjected to heat treatments at 450°C and 550°C for 1 hour in Argon gas environment. A temperature of 550°C was specially chosen to test the current material beyond conditions already reported in the literature [10,17]. Another specimen was prepared under identical conditions but without the PDC particles and tested at 550°C for 1 hour in Argon gas environment for comparison. The microstructure of each specimen was analyzed before and after the heat treatment at the same location using electron backscattered diffraction (EBSD) on JEOL 6500F. However, the electropolishing prior to the scan for the heat-treated specimen removed a few micron thickness resulting in a new surface for the scan. Scanning electron microscope (Zeiss Supra 40) and transmission electron microscope (Philips CM 200) were also utilized to observe the microstructures. The hardness tests before and after the heat treatments were performed using a Zwick-Roell ZHV1 equipment.

Fig. 1 (a) shows the inverse pole figure (IPF) map of the parent material before performing FSP. It can be seen that the grains were large and nearly equiaxed, typical of a recrystallized

microstructure. Fig. 1 (b) shows the distribution of the grain size in the parent material. It can be observed that the highest fraction of the grains was between 10 to 20 μm, and the maximum size with the lowest fraction was around 150 μm.

Fig. 2 (a) is the IPF map showing the microstructure of the FSP-obtained nugget zone before the heat treatment at 450°C for 1 hour. As can be seen, FSP produced a fine-grained microstructure with equiaxed grains. There was drastic grain refinement during the processing. The histogram for the grain size distribution is shown in Fig. 2 (b); the average measured grain size was  $1.0 \pm 0.74$  μm (number fraction-weighted). The IPF map of the exactly same area after heat treatment is shown in Fig. 2 (c). The microstructure looked very similar even after heat treatment. It was not identical to the one before heating because of the removal of a thin layer before the second EBSD measurement. The grain size distribution histogram after heat treatment is plotted in Fig. 2 (d). The average grain size was  $0.96 \pm 0.71$  μm, which was similar to the non-heat-treated condition. This shows that there was minimal change in the average grain size for this material, even after exposing it to such high temperature.

Experiments were conducted at an even higher heat treatment temperature. Fig. 2 (e) is the IPF map before the heat treatment at 550°C for 1 hour. The grain size distribution in Fig. 2 (f) shows the same initial average grain size of  $1.0 \pm 0.71$  μm (same material state as for the lower temperature heat treatment). The microstructure of the specimen after heat treatment is shown in Fig. 2 (g). It is again observed that the microstructure looked very similar to the non-heat-treated condition. The average grain size after the heat treatment was  $1.0 \pm 0.72$  μm, which was the same as that before the heat treatment. The grain size distribution (Fig. 2 (h)) was very similar to the specimen heat-treated at 450°C. Also, a closer observation of Fig. 2 (g) shows that grains with similar orientation did not coalesce. This result demonstrates the large resistance to grain growth in this material even at such a high temperature (solidus temperature of Al 5052 is 607°C).

Abnormal grain growth (AGG) is known to occur during the thermal treatments of friction stir processed Al alloys [18,19] (especially when grain boundary disorientations are small). Moreover, AGG has also been observed in other materials that have supposedly a stable grain structure due to particle pinning [20,21]. In such situations, some regions may exhibit no change in grain size, whereas others might show drastic grain growth. Hence, it was imperative to check all the regions in the nugget zone to ensure that such a scenario was not prevalent. Figs. 3 (a-i) show the backscattered electron (BSE) micrographs obtained using a scanning electron microscope (SEM) from different regions in the nugget zone of the specimen with PDC particles heat-treated at 550°C for 1 hr. The reference for the location of each BSE micrograph is schematically represented in Fig. 3 (I). It can be observed from the SEM micrographs that AGG did not occur in any of the examined regions which proves that the microstructure was stable throughout the whole nugget zone, even at 550°C. Figs. 3 (j-n) show the BSE micrographs after heat treatment at 550°C for 1 hr, for a specimen prepared under identical conditions but without the PDC particles. Fig. 3 (II) is a schematic representation of its nugget zone that serves as a reference for the locations of BSE micrographs shown in Figs. 3(j-l). It can be observed from these figures that AGG occurred in this specimen when tested under the same conditions.

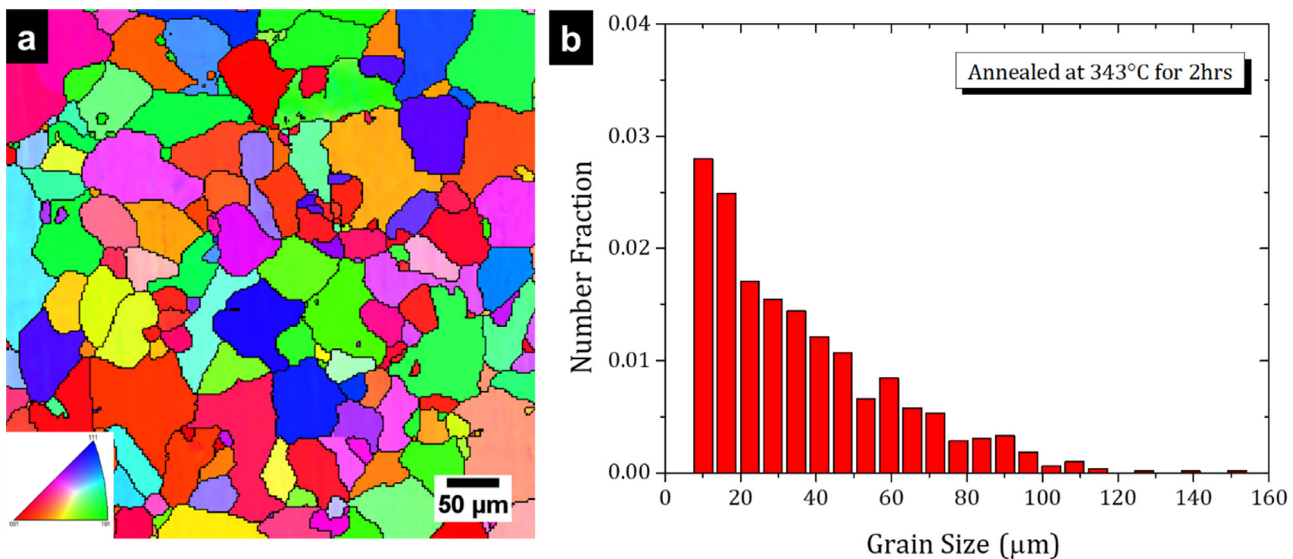


Fig. 1. (a) IPF map of the parent material. (b) The initial grain size distribution of the parent material.

As mentioned earlier, dispersion of second phase particles in the matrix applies a retarding force/drag on low and high angle grain boundaries and this has effects on recovery, recrystallization, and grain growth. The drag pressure ( $P_z$ ) from a random distribution of particles in the Zener pinning mechanism by which the grain boundary motion is inhibited by particles pinning is expressed as [9]:

$$P_z = \frac{3f\gamma}{2r} \quad (1)$$

where  $r$  and  $f$  are the radius and volume fraction of the reinforcing particles, respectively and  $\gamma$  is the boundary energy per unit area. Zener pinning is active when the particle size is less than the grain size. The maximum grain size limit ( $D$ ) until the Zener pinning can be operational is given by [22]:

$$D = \frac{4r}{3f} \quad (2)$$

Analyzing the SEM micrographs with the ImageJ software,  $r$  and  $f$  were 57 nm and 0.025, respectively, for which the limiting grain size  $D$  was calculated as 3  $\mu\text{m}$ . As the measured grain sizes were well below this value, the operation of the Zener pinning mechanism is confirmed in the current specimen.

In Fig. 4, the TEM bright-field images of the specimen before heat treatment (550°C, 1 hr) are shown. It can be observed in Fig. 4 (a-g) that nanoparticles were distributed throughout the specimen. These nanoparticles did not show any change in the diffraction contrast with respect to different tilt positions. Such a characteristic is generally exhibited by amorphous domains. Since the pre-ceramic PMHS polymer is known to convert into amorphous SiOC (PDC) after pyrolysis [23], and because PMHS is the only source for such amorphous particles in this system, it can be presumed that those nanoparticles were SiOC ceramic particles. The nanoscale size of the PDC can be obtained as the preceramic polymer can be easily fractured during FSP before the pyrolysis stage. Hence, the PDC particles can be expected to be in a size range comprising the micron to the nanoscale (as it is unlikely that fracturing during FSP will produce only nanoparticles). At higher magnifications (Fig. 4 (h) and 4 (i)), PDC nanoparticles at the grain boundaries (marked by yellow boxes) can be clearly observed. The presence of such nanoparticles can impart large drag forces to the grain boundaries and hence, impede their motion when exposed to higher temperatures.

In the TEM images (Fig. 4 (a-g)), sub-micron particles were also observed, albeit far lower in number compared to the nanoparticles. Such particles could have been contributed from the impurities present in the matrix, and they could also be PDC particles. As mentioned above the total particle volume fraction was 2.5%, the impurities (Table 1) add up to ~0.5% after conversion to volume percentage so the PDC particles were present at about 2% volume fraction. The impurity-particles had no role in the grain boundary pinning, as it was observed in the SEM micrographs in Fig. 3(j-n) that AGG occurred in the specimen that did not contain PDC particles despite having sub-micron particles distributed throughout the nugget zone. Hence, it is clear that the reason for the specimen to show grain stability at 450°C and 550°C was due to the presence of PDC particles. Part of these particles were located at the grain boundaries, while the remaining part was within the grains. Even if some boundaries did not contain PDC particles, their migration could be stopped by the particles situating within the grains. Additionally, it is also possible that the amorphous nature of the pyrolyzed PDC particles gave superior interfacial strength between the particles and the matrix. This would also increase the strength of pinning of grain boundaries by the particles. Note also that the possible  $\beta$  intermetallic phase ( $\text{Mg}_5\text{Al}_8$ ) had no contribution at all to Zener pinning as the Mg was fully in solid solution at the processing temperature (~435°C to 500°C) as well as during heat treatments (550°C and 450°C).

Grain stability up to 550°C was successfully achieved, however, the stability in the mechanical properties must also be verified. In this regard, micro Vickers hardness tests were performed before and after the heat treatments. The hardness before the heat treatment was  $76 \pm 0.764$  HV and after the heat treatments at 450°C and 550°C were  $74 \pm 0.471$  HV and  $72 \pm 0.373$  HV, respectively. Hence, from the hardness values, it can be inferred that the strength of the material changed very slightly even after exposure to such high temperatures. Kumar et al. [10] have shown that for a friction stir processed 5086 Al alloy, the grains are stable up to 250°C and the specimen exhibits AGG when exposed to 350°C for 1 hr. However, in the same work, it was observed that a friction stir processed and aged twin roll cast Al-Mg-Sc alloy exhibits considerable grain growth only when exposed to 550°C for 1 hr.

In summary, grain stability has been imparted to Al 5052 alloy till 550°C by the presence of PDC particles using the FSP process. The loss in hardness was only 5.3% after heat treatment at 550°C. Therefore, the material maintained stable microstructure

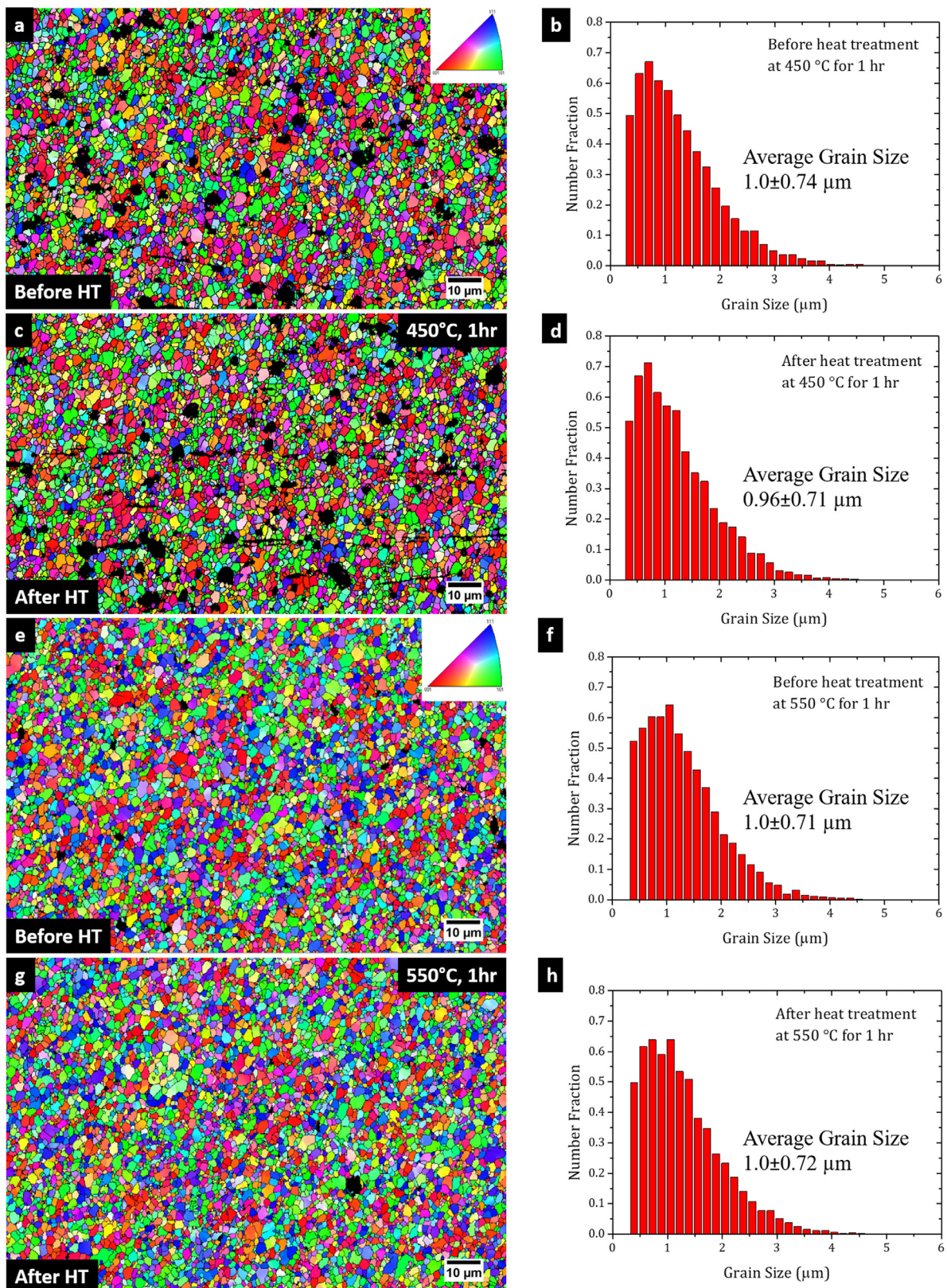


**Fig. 2.** (a) IPF map of the specimen before heat treatment at 450°C for 1 hr. HT stands for heat treatment. The black regions in the IPF map are non-indexed areas where some large particles were present. (b) The grain size distribution before the heat treatment. (c) IPF map of the specimen after the heat treatment. (d) The grain size distribution after the heat treatment. (e) IPF map of the specimen before heat treatment at 550°C for 1 hr. (f) The grain size distribution before the heat treatment. (g) IPF map of the specimen after the heat treatment. (h) The grain size distribution after the heat treatment.

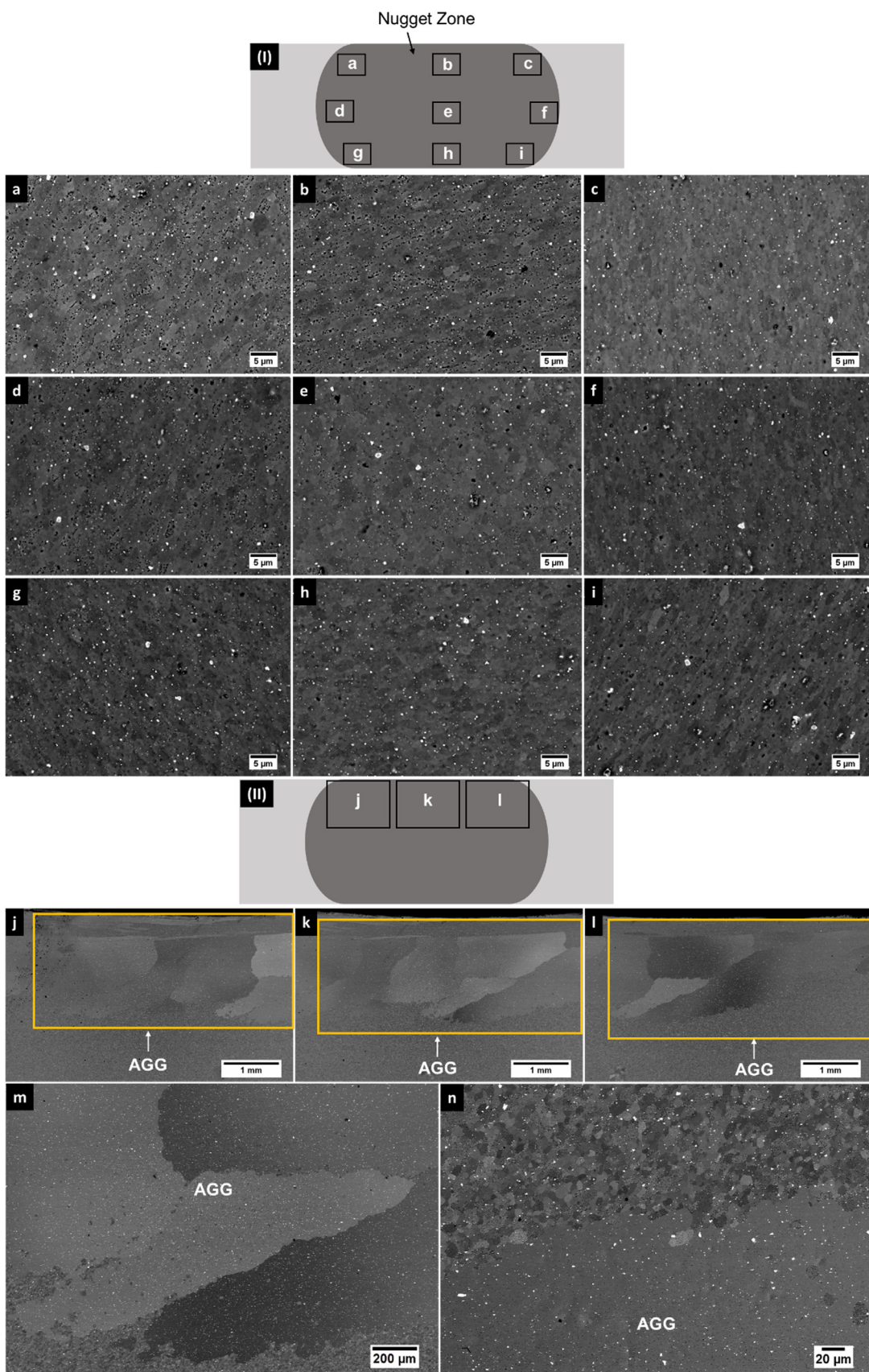


**Fig. 3.** (I) Schematic representation of the nugget zone for reference showing the location of each SEM-BSE micrograph of the specimen containing PDC particles heat-treated at 550°C for 1 hr. The corresponding SEM-BSE micrographs for each region: (a) Top-left (b) Top-central (c) Top-right (d) Middle-left (e) Middle-central (f) Middle-right (g) Bottom-left (h) Bottom-central (i) Bottom-right. (II) Schematic representation of the nugget zone for reference showing the location of each SEM-BSE micrograph of the specimen without PDC particles heat-treated at 550°C for 1 hr. The corresponding SEM-BSE micrographs for each region: (j) Top-left (k) Top-central (l) Top-right. (m) and (n) SEM-BSE micrographs at higher magnifications showing AGG in the specimen without PDC particles after heat treatment at 550°C for 1 hr.

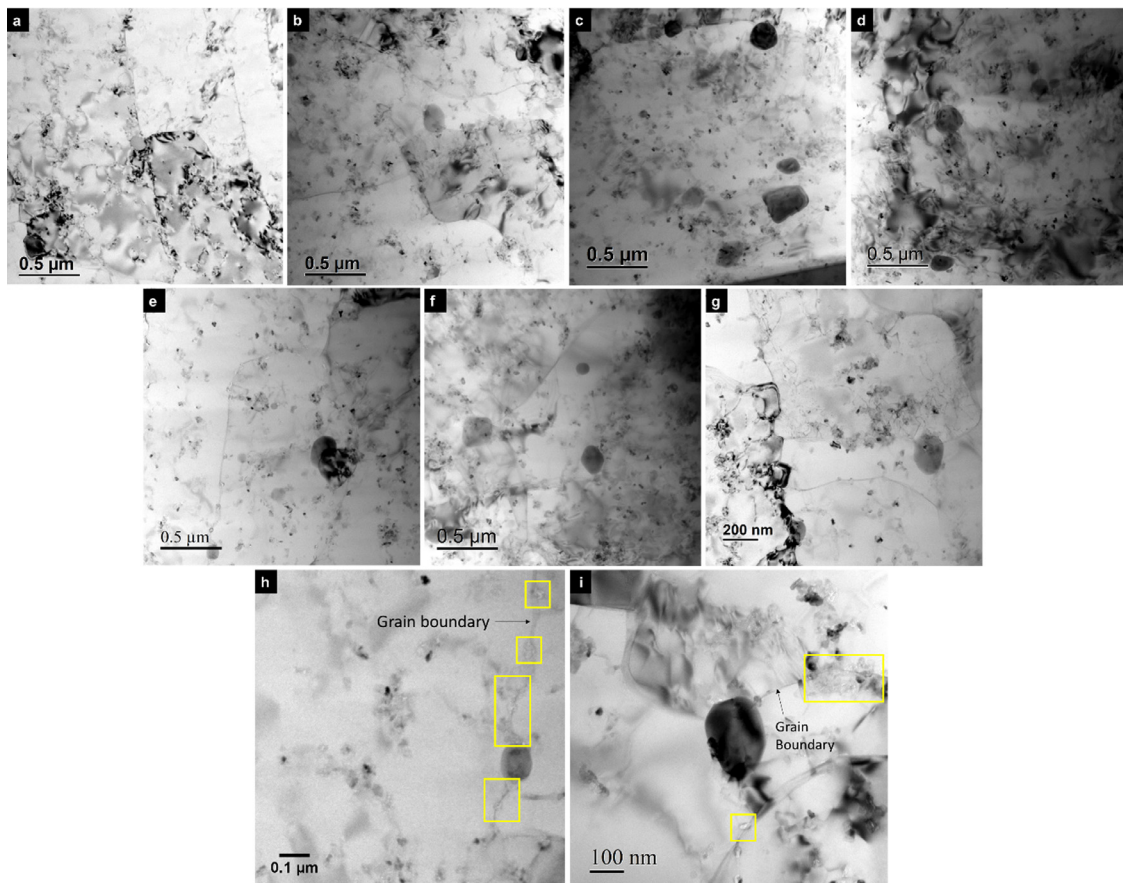


**Fig. 4.** (a-g) Low magnification bright-field images showing the nanoparticles and sub-micron particles. (h) and (i) Bright-field images at higher magnifications showing the nanoparticles at the grain boundary.

and strength during the thermal cycle. The reason for such behavior was due to grain boundary pinning by the in-situ formed PDC particles. Since the material was fabricated using FSP, verification for AGG was also performed, and was found that there was no AGG throughout the nugget zone where the particles were dispersed. However, a specimen prepared under identical conditions, but without the PDC particles, exhibited AGG at 550°C.

#### Declaration of Competing Interest

The authors declare that they have no known competing financial interests or personal relationships that could have appeared to influence the work reported in this paper.

#### Acknowledgements

This work was supported by the French State through the program “Investment in the future” operated by the National Research Agency (ANR) and referenced by ANR-11-LABX-0008-01 (LabEx DAMAS). Abhishek Pariyar acknowledges the Ph.D. scholarship awarded by the Ministry of Human Resource Development, Govt. of India. Also, special thanks to Dr. Yudong Zhang (LEM3, Labex-DAMAS, Metz, France) for the help provided during TEM operation and its data analysis. Thanks also to Dr. Julien Guyon (LEM3, Labex-DAMAS, Metz, France) for the help provided during SEM operation. A special appreciation and thanks to Dr. Chandra Shekhar Perugu (Department of Materials Engineering, IISc Bangalore, India) for discussions.

#### References

- [1] J.G. Kaufman, *Introduction to Aluminum Alloys and Tempers*, first ed., ASM International, 2000.
- [2] R.D. Bourkhani, A.R. Eivani, H.R. Nataeghi, *Compos. B Eng.* 174 (2019) 107061.
- [3] A.L. Kearney, in: *ASM Handbook, Properties and Selection: Nonferrous Alloys and Special-purpose Materials*, first ed., ASM International, 1990, pp. 152–177.
- [4] L. Ceschinini, A. Dahle, M. Gupta, A.E.W. Jarfors, S. Jayalakshmi, A. Morri, F. Rotundo, S. Toschi, R.A. Singh, *Aluminum and Magnesium Metal Matrix Nanocomposites*, first ed., Springer, Singapore, 2017.
- [5] B. Baradarani, R. Raiszadeh, *Mater. Des.* 32 (2011) 935–940.
- [6] A.B. Pandey, *High Strength L12 Aluminum Alloys*, US7909947B2 (2011).
- [7] E.O. Hall, *Proc. Phys. Soc. B* 64 (1951) 747–753.
- [8] N.J. Petch, *J. Iron Steel Inst.* 174 (1953) 25–28.
- [9] F.J. Humphreys, M. Hatherly, *Recrystallization and Related Annealing Phenomena*, second ed., Elsevier, Oxford, 2004.
- [10] N. Kumar, R.S. Mishra, *Mater. Charact.* 74 (2012) 1–10.
- [11] R. Abbaschian, R.E. Reed-Hill, *Physical Metallurgy Principles*, fourth ed., Cengage Learning, Stamford, 2008.
- [12] F.J. Humphreys, W.S. Miller, M.R. Djazeb, *Mater. Sci. Tech.-Lond.* 6 (1990) 1157–1166.
- [13] S. Deb, S.K. Panigrahi, M. Weiss, *Mater. Charact.* 154 (2019) 80–93.
- [14] P. Ajay Kumar, R. Raj, S.V. Kailas, *Mater. Des.* 85 (2015) 626–634.
- [15] P. Colombo, G. Mera, R. Riedel, G.D. Sorarù, *J. Am. Ceram. Soc.* 93 (2010) 1805–1837.
- [16] R.S. Mishra, Z.Y. Ma, I. Charit, *Mater. Sci. Eng. A* 341 (2003) 307–310.
- [17] I. Charit, R.S. Mishra, M.W. Mahoney, *Scr. Mater.* 47 (2002) 631–636.
- [18] I. Charit, R.S. Mishra, *Scr. Mater.* 58 (2008) 367–371.
- [19] S. Jana, R.S. Mishra, J.A. Baumann, G. Grant, *Mater. Sci. Eng. A* 528 (2010) 189–199.
- [20] J.E. May, D. Turnbull, *Trans. AIME* 212 (1958) 769–781.
- [21] E.A. Holm, T.D. Hoffmann, A.D. Rollett, C.G. Roberts, *IOP Conf. Ser.: Mater. Sci. Eng.* 89 (2015) 012005.
- [22] P. Bate, *Acta Mater.* 49 (2001) 1453–1461.
- [23] S. Nedunchezian, R. Sujith, R. Kumar, *J. Adv. Ceram.* 2 (2013) 318–324.